Journal of Andrology, Vol. 26, No. 1, January/February 2005

Particle Distribution in Low-Volume Capillary-Loaded Chambers

DIARMAID H. DOUGLAS-HAMILTON,* NANCY G. SMITH,* CHRISTOPHER E. KUSTER,† JAN P. W. VERMEIDEN,‡ AND GARY C. ALTHOUSE§

*From *Hamilton Thorne Biosciences, Beverly, Massachusetts; †Kuster Research and Consulting, Geneseo, Illinois; ‡IVF Center, Department of Reproductive Medicine, VUMc Academic Hospital, Vrije Universiteit, HV Amsterdam, The Netherlands; and §the University of Pennsylvania, School of Veterinary Medicine, Department of Clinical Studies—New Bolton Center, Kennett Square, Pennsylvania.*

ABSTRACT: Accurate determination of sperm concentration in fluid suspension is a critical component in a semen analysis. Inaccurate estimations can lead to misinterpretation of the spermiogram and, in the case of livestock production, can lead to faulty insemination doses, which can adversely affect stud power, fertility, fecundity, and cost effectiveness of breeding programs. Capillary-loaded slides, like the hemacytometer, have been the standard for calibration of other concentration estimation modalities such as photometry, Coulter counter, flow cytometry, and computer-automated semen analysis (CASA). Single-use capillary-loaded slides, much smaller than the hemacytometer, are frequently used by many of the current CASA systems. As the use of CASA increases, more field reports are suggesting differences between CASA results and hemacytometry. In this article, we establish that these differences are, in large part, due to the Segre-Silberberg effect, which occurs during Poiseuille flow in high-gradient fluid flow in thin capillary-loaded slides. We develop the theory of this phenomenon and derive the scaling and significance of the effect. Finally, we graphically provide a means for predicting the necessary compensation factor when using capillary-loaded slides to determine sperm concentration.

Key words: Spermatozoa, concentration, capillary slide, hemacytometer, Poiseuille, Segre-Silberberg.

J Androl 2005;26:107–114

In many applications, it is often necessary to determine the concentration of particles (eg, cells) in fluid suspension. During semen analysis, accurate determination of sperm concentration in an ejaculate is a critical component of the spermiogram and, in the case of livestock, necessary for optimizing calculable insemination dose numbers. If inaccurate estimations are generated, along with faulty interpretation of the spermiogram, faulty insemination doses can jeopardize ejaculate optimization, fertility, and fecundity.

Sperm concentration is determined by a number of methods, most of which have roots in their calibration via hemacytometry. Popular methodologies today include determining attenuation of an optical beam from light scattering or absorption in the sample (eg, photometry), by counting cells individually in a restricted-flow apparatus (eg, Coulter counter, flow cytometry), or as with hemacytometry, by placing the sample in a chamber of known volume and counting cells individually (eg, computer-automated semen analysis systems [CASA]). For CASA, a small-volume slide of narrow depth is desired, which provides for a monolayer of cells while not impeding sperm swimming motion as well as for providing appropriate focal depth to clearly image the specimen throughout the chamber. For most specimens, a chamber of 20 μm in depth works well, with these slides designed to fill by capillary action.

Capillary flow into a 20-μm chamber follows a classical laminar Poiseuille flow. The fluid flow is viscosity dominated and exhibits maximum velocity halfway between the chamber walls, decreasing to 0 at the chamber walls. The velocity gradient produces a transverse lifting force on suspended particles, with the force driving particles toward 2 stable planes situated a short, calculable distance from the walls. This phenomenon has been previously described and is known as the Segre-Silberberg (SS) effect (Segre and Silberberg, 1961). The result of this SS effect is that particles are drawn from the flow edges into faster flowing layers of the fluid, causing cell-concentration changes within the chambered flow. To better understand these flow dynamics, we developed a model of the problem of particle segregation effects in capillary-loaded chambers. This model predicts how long it takes for transverse particle motion across the flow to become significant, how rapidly variations in particle concentration develop in the chamber and provides a numer-

Correspondence to: Gary C. Althouse, University of Pennsylvania, School of Veterinary Medicine, Department of Clinical Studies, New Bolton Center, Kennett Square, PA 19348-1692 (e-mail: gca@vet.upenn.edu).

Received for publication May 25, 2004; accepted for publication September 8, 2004.

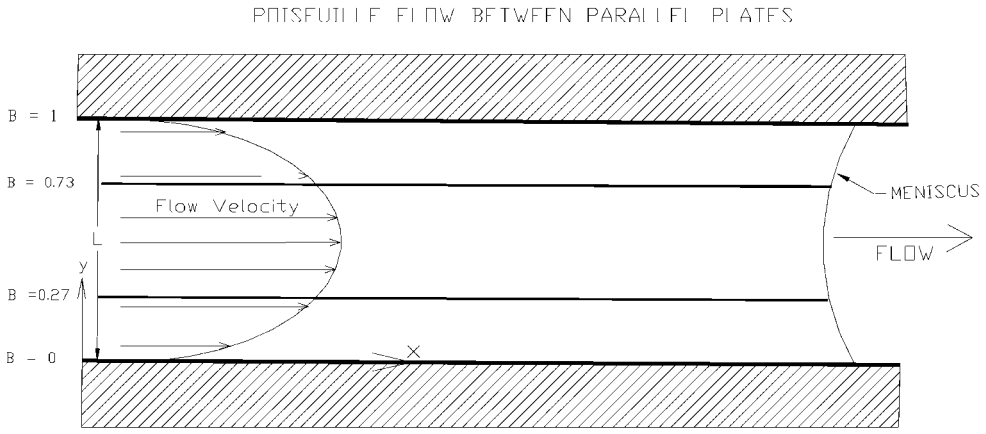

Figure 1. Capillary Poiseuille flow between 2 plates. Dimensions *y* is transverse, *x* is parallel to flow. Values of β given as B. The two SS planes are indicated at B = 0.27 and B = 0.73.

ical estimate for the degree of concentration changes that can be anticipated.

Theoretical Model

Poiseuille Flow—Poiseuille flow describes laminar flow in a tube or between parallel sheets. In the present case, the latter is of most interest because it is exactly the flow type that occurs when a sample is loaded into a capillary chamber. For modeling, we have selected a 4-chamber 20-μm linear flow slide (Leja Products B. V., Nieuw Vennep, Amsterdam, The Netherlands). We will initially summarize classical Poiseuille flow between two parallel sheets. Defining fluid density as ρ, velocity as *U*, characteristic length as *L*, and viscosity μ, the Reynolds number is Re = ρ*UL*/μ. When a system is characterized by low Reynolds number (Re < 1), laminar Poiseuille flow results (Daily and Harleman, 1966).

Define *x* to be the direction of flow, *y* to be the direction perpendicular to the walls, and *L* to be the wall spacing. Assume the transverse width of the chamber is very much greater than the chamber depth, so that the width is effectively infinite. The dimensionless distance across the channel is defined as β = *y*/L. Then the fluid velocity *U* at any distance *y* from the wall is given by

$$U = 4U_m(\beta - \beta^2) \tag{1}$$

where the peak central velocity at β = ½ is U_m. The flow is shown in Figure 1, and values of β are indicated as B.

Flow Velocity Under Surface Tension—For surface tension force, $S = S_0\cos\theta$, drawing fluid into the chamber, where S_0 is the surface tension between fluid and glass and θ is the contact angle. After the fluid has traveled a distance *x* into the chamber, the pressure gradient will be

$$\frac{dp}{dx} = \frac{2S}{Lx}, \tag{2}$$

where *p* is the pressure, and the factor 2 is used because there are 2 surfaces separated by distance *L*.

The peak velocity and the mean bulk velocity are given respectively by

$$U_m = \frac{L^2}{8\mu}\frac{dp}{dx} = \frac{1}{4}\frac{SL}{\mu x} \quad \text{and} \quad \bar{U} = \frac{2}{3}U_m \tag{3}$$

where the viscosity μ is independent of velocity and the pressure gradient is the driving force of the capillary flow. Flow velocity increases to a maximum at the center of the channel (β = 0.5), is parabolic in β, and decreases linearly with the meniscus penetration distance *x*. The fluid velocity will be maximal at entry, proportional to chamber depth, and decrease as the meniscus proceeds into the chamber. During fluid penetration, the transverse velocity gradient will slowly decrease. Logically then, from Equation (3), wider chambers such as the hemacytometer (100 μm) should fill proportionately more rapidly than narrower (20 μm) chambers, as in fact they do.

Transverse Motion—It was first reported by Segre and Silberberg (1961) that particles suspended in a Poiseuille flow become concentrated at a well-defined distance from the walls. This preference of the particles for a certain wall distance applies both to cylindrical and planar Poiseuille flow. In this early work, Segre and Silberberg found that, in tubes, the preferred position was 2/3 of the radius, while, for rectangular flows, it was at approximately β = 0.167 of the plane separation (because the flow is symmetric, there is a corresponding position at 0.863 near the other wall: in the following we will consider just the region from first wall to centerline). Shekriladze (1982) provided a first-principles derivation of the preferred position in the SS effect. Further experimental work has shown that particles collect at a position dependent on particle size and flow conditions. Analytical results for the case of slow-flow, small particles between

plane walls (Vasseur and Cox, 1976) and finite-element numerical analyses for larger particles and higher Reynolds numbers (Feng et al, 1994) have both shown that spherical particles congregate close to a stable position at $\beta_0 = 0.265$–0.275. This position is indicated in Figure 1.

The exact value of β_0 depends on whether the particles are free to rotate, as well as on particle size and shape. For sperm, which may be approximated as nonrotating ellipsoids with a tail rather than as spheres, the stable position may be slightly different than that of a sphere, but nevertheless, will be a stable position.

We will conservatively adopt the value $\beta_0 = 0.265$ as the position of the stable SS plane. We will assume that the same value applies to sperm and derive the effect on sperm concentration in laminar Poiseuille flow. Agreement with experimental results (Douglas-Hamilton et al, 2005) confirm that this is a justifiable assumption.

Particles Are Pumped Toward the Meniscus—In Poiseuille flow, according to Equations (1) and (3), the flow velocity is the same as the mean fluid flow speed at $\beta = \beta_m$, where $\beta_m = 0.211$ (and at the symmetrical position, $\beta_m' = 0.789$). If particles collect in regions where $\beta_m < \beta < \beta_m'$, they will move more rapidly than the mean fluid flow. If this occurs, the particles will be entrained at almost the same velocity as the local fluid because slip between fluid and particle is small and will end up moving more rapidly than the mean fluid velocity. The SS plane is at $\beta_0 = 0.265$ and $\beta_0 > \beta_m$, so the particles move more rapidly than the average and, thus, will be transported to the leading edge of the flow. This implies that they will form a wave of higher concentration at the meniscus, where Poiseuille flow is not fully developed and the velocity gradients are not yet formed.

Dependence on Gradient and Chamber Depth—From the analysis of Vasseur and Cox (1976), transverse particle velocity varies as the square of the transverse fluid velocity gradient and is greatest in the regions with highest gradient near the walls. Consequently, in the central regions, where the gradient is low, the transverse velocity is greatly reduced. For present purposes, we will henceforth neglect the transverse motion in the central flow regions because the gradient is negligibly small and, thus, consider only the transport of particles from the region $\beta < \beta_0$, near the wall, toward the stable position $\beta = \beta_0$.

Note that, from Equation (3), the velocity gradient is proportional to $U_m/L = S/4\mu x$ and, therefore, is independent of chamber depth. Consequently, the transverse cell velocity is similar in chambers of different depths, the difference being that, in the deeper chambers, cells will take proportionately longer to migrate to the stable position $\beta = \beta_0$.

Laminar Flow SS Transverse Velocity and Concentration Reduction—Vasseur and Cox (1976) made a valuable analytic examination of small rigid spheres entrained in Poiseuille flow at low Reynolds number. Their assumptions were that the Reynolds number was $\mathrm{Re} < 1$ and that the particles were small compared with the separation between the walls. By these assumptions, particles could be treated as point objects subjected to a point force in the flow gradient either if freely rotating or constrained against rotation.

Sperm probably fall between these extremes because the tail must retard rotation in the gradient, although it should not completely prevent it. Sperm heads are not spherical and predicting their behavior would require a detailed finite element analysis of the type done by Feng et al (1974), where they treated elliptical objects in laminar flow at high particle Reynolds number. Given these considerations, the Vasseur and Cox treatment can still provide a good analytical indication of small particle (eg, sperm) behavior in Poiseuille flow.

If the SS effect is incompletely developed during the flow, the velocity of particles transverse to the flow direction integrated over the flow duration will determine how much concentration difference will exist. On the other hand, if we can approximate the SS effect as fully developed, the concentration difference is given by a simple analytic expression, which is derived below.

Development of SS Effect

If we use pig sperm as an example, the sperm head surface area (Roberts, 1986) is approximately that of a sphere of radius $a \sim 2$ μm. For neutral-density spherical particles of this radius entrained in a fluid of density ρ and viscosity μ into a capillary chamber of width $L = 20$ μm, we have $\mathrm{Re} \sim 0.02$, and $\kappa = a/L \sim 0.2$, so the flow is laminar and Vasseur and Cox's assumptions of small κ and Re are valid. We will adopt their analytic results for the transverse velocity of a (nonrotating) particle of radius a with the same density as the fluid, in a Poiseuille flow with central velocity U_m. We define the downstream direction as x and the transverse direction as y, as in Figure 1.

Using a Fourier transform technique, Vasseur and Cox (1976) derived the transverse velocity in the y-direction as

$$V_y = \frac{a\rho U_m^2}{\mu}\left(\frac{a}{L}\right)^2 F \tag{4}$$

where U_m is the central downstream flow velocity and F is a dimensionless function of position in the y-direction. The transverse velocity is therefore proportional to the square of the downstream velocity gradient U_m/L, which implies, from Equation (3), that V_y is independent of the chamber depth. The result of numerical integration, F can be approximated as

$$F = b_0 + b_1\beta + b_2\beta^2 \tag{5}$$

where the numerical constants are $b_0 = 1.652$, $b_1 =$

-9.6493, $b_2 = 12.8929$, so V_y is fully defined. Note that F has a root at $\beta_0 \sim 0.265$. We will use the approximation for F only in the region where $\beta < \beta_0$. Although the numerical value of F depends on particle shape and rotation, the form of Equation (4) is functionally independent of them. The results obtained should be qualitatively valid even if the numerical values depend on uncertain parameters.

Particle Trajectory

Slip between particle and fluid is small in viscosity-dominated flow. Neglecting slip, we can now define the particle trajectory as that needed to keep true the condition

$$\frac{dy}{dx} = \frac{V_y}{U}. \tag{6}$$

Substituting Equations (1), (3), and (4) into (6), using $y = L\beta$ and collecting all the constants, we define the dimensionless figure of merit parameter K,

$$K = \frac{Sa^3\rho}{16\mu^2 L^2} \tag{7}$$

and Equation (6) becomes

$$\frac{d\beta}{dx} = K\frac{1}{x}\frac{F}{\beta - \beta^2}. \tag{8}$$

The trajectory of a particle will be the integral of Equation (8), taken from initial conditions $x = \delta$, and $\beta = \beta_1$, say, and over the range $0 \le \beta_1 < \beta \le 0.265$. Here, $x = \delta$ represents the distance into the flow at which Poiseuille flow is developed, and $\beta = \beta_1$ is the initial transverse position in the flow from which the particle begins at $x = \delta$. This integral will give the track of a particle in (x, β) coordinates as it moves rapidly down the flow in the x-direction and slowly across the flow in the y- (or β-) direction. We can integrate Equation (8) over the range from $\delta = 0.1$ cm up to x, and from $\beta = \beta_1$ up to the final value β at position x. The particles will tend to collect near the SS plane, $\beta = \beta_0$, given enough time: we wish to estimate how much time is required to get significant transverse motion of particles in the flow and thus how much separation and differential concentration will result.

Integration of the Trajectory

Integration of Equation (8) gives the trajectory of the particle in (β, x) coordinates as

$$x = \delta e^{[I(\beta) - I(\beta_1)]/K} \tag{9}$$

in which

$$I(\beta) = -\frac{\beta}{b_2} + \frac{b_1 + b_2}{2(b_2)^2}\ln F + \frac{-(b_1)^2 + 2b_2b_0 - b_2b_1}{2(b_2)^2 G}\ln\left(\frac{2b_2\beta + b_1 - G}{2b_2\beta + b_1 + G}\right)$$

with $G = \sqrt{(b_1)^2 - 4b_0b_2}$, the numerical constants b_0, b_1, and b_2 are from Equation (5), and β_1 is the initial value of β.

Equation (9) now gives the trajectory of a particle starting at position (β_1, δ) and ending at position (β, x). We can therefore obtain the transverse position β reached at any distance x traveled along the flow. This is equivalent to obtaining final position Y from initial position y.

The downstream displacement x is exponential in a logarithmic function of β, and the rapidity of the exponential takeoff depends on K. In other words, because the transverse particle velocity in the y-direction slows down on approaching the $F = 0$ plane, the x-velocity is more dominant for higher β and sweeps the particles downstream as soon as they depart from their initial position. Over long times, all particles will collect at the y-velocity = 0 plane, where $F = 0$, at approximately $\beta = \beta_0 = 0.265$. Over the chamber length of $x = 2$ cm, which is of interest in the present case, the particle segregation at the pole will be reduced by minimizing transverse motion. In order to suppress transverse compared with parallel motion, we need to keep $K = Sa^3/(4\mu L)^2$ as small as possible. This implies reducing surface tension S (or reducing the inflow velocity), reducing radius a, increasing viscosity μ or increasing chamber depth L. Note that reducing flow rate is mathematically equivalent to reducing the driving surface tension S.

It can be seen that wider chambers will show much less SS segregation over their initial regions. Higher viscosity will correspondingly result in reduced segregation. In the next section, we apply Equation (9) to predict the trajectories and the concentration of sperm in various chambers under various conditions. In so doing, we make the assumption that the sperm can be treated as spheres of radius 2.0 μm. In practice, this approximation appears to be justified by the results.

Numerical Trajectory Results

Capillary Slide Model

The slide has chamber depth $L = 20$ μm, and the sample flows into it in about 2 seconds via capillary flow. The viscosity of diluted boar semen ($\mu = 1.2$ centipoise [cP]) approximates that of water. Using the viscosity of water, $\mu = 1.0$ cP at 20°C, and allowing for a 40° contact angle between meniscus and glass walls, we get the effective surface tension force driving the capillary loading as $S = 72 \cos 40 \approx 53$ d/cm. We take sperm head radius $a = 2$ μm and get $K = 0.066$.

Values of x versus β are shown in Figure 2, for $K = 0.066$. We take trajectories beginning from starting points at $y_0 = 1, 2, 3, 4, 5$ μm from the wall, equivalent to initial $\beta = 0, 0.05, 0.1, 0.1, 0.2$ (off course, an identical plot

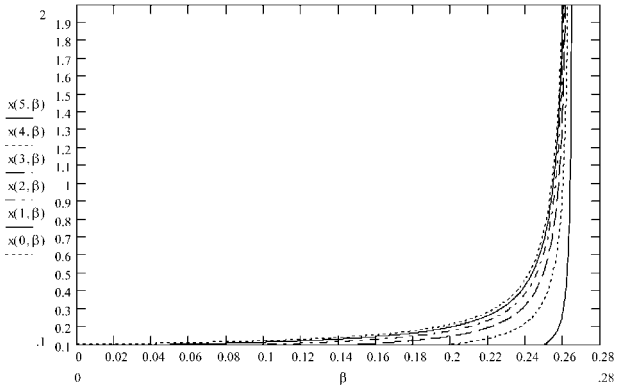

Figure 2. Computed trajectory of 4-μm-diameter particles in capillary Poiseuille flow in a 20-μm chamber. β (abscissa) is relative transverse location, and *x* (ordinate) is position in flow direction (mm from inlet). The lines indexed 0–5 correspond to initial value β = 0, 0.05, 0.01, 0.15, 0.2, 0.25, respectively. Segregation at SS plane β_0 = 0.265 is almost complete after 1 mm.

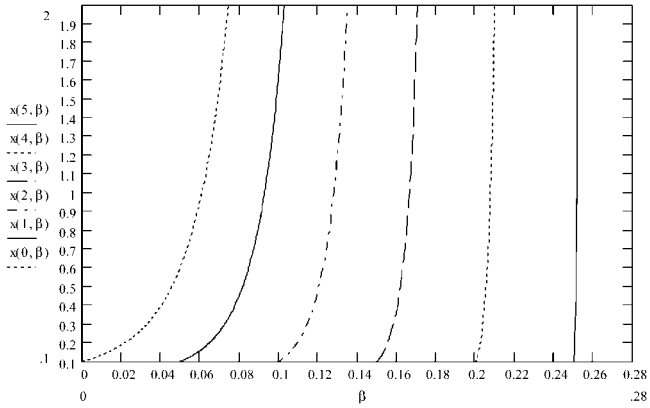

Figure 3. Computed trajectory of 4-μm-diameter particles in a hemacytometer with depth *L* = 100 μm. Segregation is barely begun at 2 mm, much slower than in Figure 2.

could be drawn from the opposite wall). The evaluations from Equation (9) are shown in Figure 2.

Treating sperm cells as having properties in the flow similar to spheres of radius 2.0 μm, sperm cells rapidly congregate at the SS plane β_0 = 0.265, and after 1 mm of flow into the chamber, they should all be within 10% of that position. In this case, one would expect a fully developed segregation of particles and a leading-edge, high-concentration wave just behind the meniscus, to form within 1 mm of entering the chamber. The sperm cell concentration will thus be reduced in the postmeniscus flow.

Hemacytometer Model

In this example, *L* = 100 μm, giving 5 times more rapid inflow than the capillary slide model and much more uniform cell distribution between the laminar flow planes in the chamber. Figure 3 shows the predicted transverse flow after Poiseuille flow has developed. It was shown (see Equation [3]) that the transverse velocity is unchanged, but the distance to travel across the chamber is 5 times greater and the time available is 5 times shorter. As a result, very little leading-edge concentration would be predicted for the hemacytometer. The effect on postmeniscus sperm concentration is derived below, and it will be seen that sperm segregation effects are predicted to be very small in a hemacytometer.

The transverse velocity is similar, but the downstream flow is much faster in the hemacytometer and the chamber is 5 times deeper, so no significant segregation appears to take place during the loading. In fact, no leading-edge concentration wave is seen experimentally in the hemacytometer. We interpret this result as due to the distance from conduit to counting grid (~3 mm) being insufficient to obtain fully developed Poiseuille flow, combined with the shorter time available and longer distance to travel before segregation becomes significant. In a longer 100-μm chamber, a slight leading-edge concentration becomes apparent after 2 cm of travel, but this is not of importance for the short (1-cm) hemacytometer chamber (Althouse et al, 1995).

Estimate of SS Effect on Particle Concentration

If particles are moved transversely into a more rapidly moving stream, their density will decrease because, while the net transport rate of particles is the same, the higher velocity means a lower concentration. Therefore, the net density of particles averaged over an area perpendicular to the fluid flow and to the plane of the chamber will be decreased by this particle transfer. The numerical magnitude of this effect is derived.

The Continuity Equation

The continuity equation describes the particle density ρ in a flow of velocity *U*

$$\frac{d\rho}{dt} + \nabla\cdot(\rho U) = 0. \tag{10}$$

In determining the concentration in the flow of particles in a rectangular channel, the particles within an area *A* are counted and the instantaneous concentration of cells within that area is obtained as number of particles divided by the known volume.

If the flow is laminar, and the concentration in the sample is ρ_0, then, barring lateral transfer effects, the count read at any position of area *A* will be $N = \bar{\rho}Ad$, where $\bar{\rho}$ is the particle density averaged along the line of sight and *d* is the chamber depth. Without lateral transfer, $\bar{\rho} = \rho_0$. And if particles are transferred from a slow-moving to

a faster moving part of the flow while the input sample density remains constant, the net total rate of all cells passing any point in the channel must be unchanged, and because the cells are moving faster, their density must be lower. Therefore the value of N must decrease and the derived value of $\bar{\rho}$ must decrease proportionally to the change in velocity of the particle-bearing stream.

In steady-state, $d\rho/dt = 0$, and, from Equation (10), we obtain $\rho U = constant$ Hence, $\rho \alpha U^{-1}$. That is, the mean observed density will be inversely proportional to the (downstream) velocity of the particle. Therefore, as the particles move into faster streamlines, their observed concentration will proportionately decrease. By computing the ratio of the new streamline velocity to the initial velocity for a given particle, and summing over all streamlines, we can estimate the new steady-state concentration measured in the flow. More exactly, we can estimate the ratio that the new measured concentration bears to the actual sample concentration.

Velocity and Concentration

Each initial particle position y is mapped into a final (downstream) particle position Y. We do not need to consider the y-velocity because it is very small compared with the x-velocity. The ratio of the initial to final x-direction velocity of a particle with initial coordinate y and final coordinate Y is then

$$r = \frac{U(y)}{U(Y)} \tag{11}$$

where U is the velocity at position y.

Integrating over all particles up to the maximum final y-position, Y_{max}, and using the continuity equation, we define the density decrement Δ as the average proportional change in apparent concentration

$$\Delta = \frac{\bar{\rho}}{\rho_0} = 1 - \frac{2Y_{max}}{L}\left(1 - \frac{1}{Y_{max}}\int_0^{Y_{max}} r\, dy\right). \tag{12}$$

In Equation (12), the second term has factor 2 because the stream is symmetrical in either wall, and the ratio Y_{max}/L is introduced because the particle transverse velocity in the central part of the flow is neglected compared with that outside the SS plane, $y = Y_{max}$. In fully developed SS flow, the particles will arrive at the SS plane.

For non–fully developed flow, the final value of the y-coordinate will not reach the SS plane. At the point of concentration measurement, the particles will have reached a position β_{final}, depending on their initial position β. We can estimate their final position by approximating $I(\beta)$ from Equation (9) as

$$I(\beta) \approx I_0 + ae^{b\beta} \tag{13}$$

where

$$I_0 = 0.05 \qquad a = 1.1189 \times 10^{-3} \qquad n = 18.7982.$$

Equation (13) gives fair qualitative agreement with the integrated value for $I(\beta)$ for the region $\beta < \beta_0$. Using Equation (13) in Equation (9), the final value of β at the final value of x becomes

$$\beta_{final} = \frac{1}{b}\ln\left\{\frac{1}{a}\left[K\ln\left(\frac{x_{final}}{\delta}\right) + I(\beta) - I_0\right]\right\}. \tag{14}$$

Here, the dimensionless position across the stream after x cm travel downstream in the flow is β_{final}, and the initial value is β. Because the final position cannot exceed $Y_{max} = L\beta_0$, substituting in Equation (12), we can derive the resulting concentration change for incomplete drift where the particles have not all arrived at the SS plane, by integrating over all possible initial values of β. The concentration decrement becomes

$$\Delta = 1 - 2\beta_0\left(1 - \frac{1}{\beta_0}\int_0^{\beta_0}\frac{\beta - \beta^2}{\beta_{final} - \beta_{final}^2}\, d\beta\right). \tag{15}$$

Thus Δ is a function of the figure of merit K and the downstream distance traveled x_{final}, values of which will be given in the following section.

Results

Numerical Predictions of Sperm Concentration in Slide

Density Decrement, Compensation Factor, and Figure of Merit K—We have defined the figure of merit as the dimensionless number given in Equation (7). We show explicitly its dependence on chamber width and fluid viscosity in Figure 4a. We can logically assume that the surface tension is $S = 53$ dyne/cm, corresponding to water-to-glass at a contact angle of 40°, and we take the size of a typical sperm cell as effectively a sphere of radius 2.0 μm. The figure of merit K is then given in Figure 4a, in which K is a function of the viscosity over the range 1 to 10 cP, which covers from water to typical human semen. The effect of chamber depth is given for values from 10 to 100 μm.

The density decrement Δ depends monotonically on the figure of merit K. The compensation factor required to obtain the true concentration from the measured concentration is $1/\Delta$. We have summarized the results from Equation (15) in Figure 4b, where the compensation factor is given as a function of K, for measurement at distances 2 and 10 mm into the chamber. Figure 4b gives the predicted compensation factor required for different chamber depths and sample viscosities.

Density Decrement Approximation—In fully developed Poiseuille flow (ie, at positions far behind the meniscus and far from the entry), transverse migration will cause

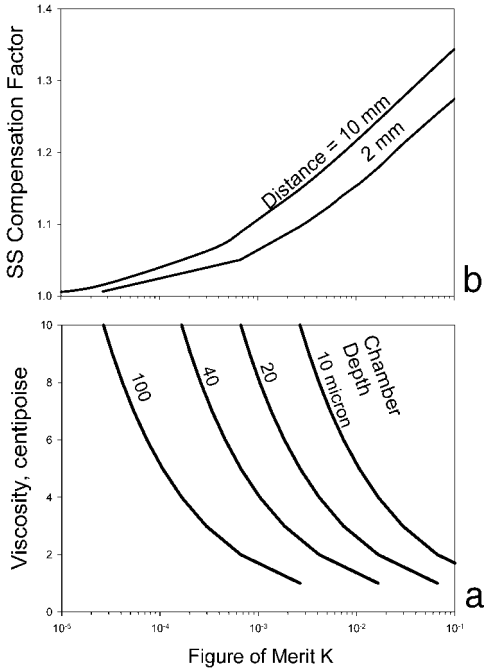

Figure 4. **(a)** Figure of merit as a function of viscosity and chamber depth for 2.0-μm-radius spheres, surface tension 53 d/cm. **(b)** Predicted compensation factor from figure of merit *K* for distance 2 mm and 10 mm from point of entry.

the observed particle concentration to be lower than that found in the original sample. The concentration is reduced in proportion to the velocity ratio between particles and mean fluid, as required by continuity. For complete development of the SS effect, all the slow-region cells are swept into the stream at (or very close to) $\beta = \beta_0$. The concentration decrement, or ratio of measured to true sample concentration, is obtained by integrating Equation (15) with $\beta_{final} = \beta_0$, and is given by the expression

$$\Delta = \frac{3\beta_0 - 2\beta_0^2}{3(1 - \beta_0)} + (1 - 2\beta_0) \tag{16}$$

Value of β_0 and Compensation Factor—We have assumed that sperm behave analogously to spheres in the flow, and migrate to the plane at $\beta_0 \sim 0.265$. From Equation (16), this migration results in a concentration deficit $\Delta \sim 0.77$. The same deficit will apply to any fully developed SS effect in Poiseuille flow, so that, in any capillary-loaded chamber that is sufficiently long, the particles will collect at $\beta = \beta_0$, and the concentration decrement factor is given by (16). It is not very sensitive to the exact position of the SS plane $\beta = \beta_0$: if the SS plane is at the wall, $\beta_0 = 0$ and then $\Delta = 1$ and, if the SS plane is at the centerline, $\beta_0 = 0.5$ and then $\Delta = 2/3$, as expected. For low-viscosity samples, such as diluted boar semen in 20-μm chambers, the SS effect is almost fully developed within 2 mm. We expect, therefore, that, for low-viscosity samples, $\beta_0 = 0.265$, and the measured concentration at 10 mm from the entry in a 20-μm chamber will be approximately 77% of the true sample concentration. The compensation factor will therefore be $1/\Delta = 1.30$.

For viscous samples, the effect is not fully developed in 10 mm and the effect on concentration is predicted from Equation (15), shown in Figure 4. The prediction is that high viscosity reduces the SS effect and the required concentration compensation factor. For human semen with viscosity 7–8 cP (Gonzalez-Estrella et al, 1994) in a 20-μm chamber, one would require approximately 10% compensation. For diluted porcine semen with viscosity approximately 1.2 cP, one would require approximately 30% compensation. This compensation factor 1.3 should be applied when the sperm concentration is counted or measured in a 20-μm capillary-loaded chamber and the sperm suspension is of low viscosity.

Hemacytometer—The speed of transverse movement, like the velocity gradient, is independent of the slide-chamber depth. Consequently, cells in the 5 times wider 100-μm hemacytometer will take 5 times longer to reach the SS position than in the 20-μm slide. At the same time, Poiseuille flow will take longer to become established in the hemacytometer. Experimentally, the SS segregation effect is not seen in the hemacytometer, probably because loading times are short in the small chamber, the observation region is close to the loading port, and the Poiseuille flow and SS effect are not fully developed at the position where the sample is examined. Therefore, the hemacytometer remains the gold standard for measuring particle concentration in fluids.

Discussion

In the 20-μm-depth chamber, for low-viscosity samples such as diluted animal semen (eg, porcine, equine, bovine) used in breeding, the slower cells rapidly reach the SS position, resulting in a mean increase in their downstream velocity. Due to transport into faster moving layers, the average sperm downstream velocity in the slide will be about 1.3 times the average fluid velocity. This increase in mean velocity results in the concentration per unit area of the slide being about $1/1.3 \cong 77\%$ of the true hemacytometer concentration measurement. If sperm follow the same principles as observed with perfect spheres, we would therefore expect the typical slide measurement to be lower than the true sample concentration in that ratio. In practice, sperm may have a different stable SS position due to their complex shape, and the resultant concentration ratio may be different; however, experimental results with diluted swine semen (Douglas-Hamilton et al, 2005) agree well with the fully developed SS effect case as described.

In conclusion, we propose that particle segregation in

Poiseuillle flow must be taken into account when using thin, low-volume capillary-loaded slides in order to obtain an accurate estimation of sperm concentration. For low-viscosity, diluted animal semen concentration measurement in 20-μm slides, a predicted compensation factor of 1.30 would have to be applied to obtain the actual sample concentration. Provided the SS effect is complete, Equation (16) is valid and the concentration change is independent of suspended particle dimensions. This will be the case for low-viscosity specimens with $\mu \sim 1$. In high viscosity samples, such as unwashed human semen, the inflow rate is reduced and in general the SS effect will not be complete. The viscosity-dependent estimation from Equation (15) is then required, as given in Figure 4a and b.

Acknowledgments

We are grateful to Irakli Shekriladze for pointing out the relevance of the SS effect and to D. Katz, D. Owen, and D. Mortimer for kindly providing information on human semen viscosity.

References

Althouse GC, Bruns K, Evans LE, Hopkins SM, WH Hsu. A simple technique for the purification of ejaculated boar spermatozoal plasma membranes. *J Prep Biochem.* 1995;25:69–80.

Daily J, Harleman D. *Fluid Dynamics.* Boston: Addison Wesley; 1966: 76–80.

Douglas-Hamilton DH, Smith N, Kuster C, Vermeiden J, Althouse G. Capillary-loaded fluid dynamics: effect on estimation of sperm concentration. *J Androl.* 2005;26:115–122.

Feng J, Hu JJ, Joseph D. Direct simulations of initial value problems for the motion of solid bodies in a Newtonian fluid: Couette and Poiseuille flows. *J Fluid Mech.* 1994;277:271–301.

Gonzales-Estrella JA, Coney P, Ostash K, Karabinus D. Dithiothreitol effects on the viscosity and quality of human semen. *Fertil Steril.* 1994;62:1238–1243.

Roberts SJ, ed. *Veterinary Obstetrics and Genital Diseases (Theriogenology).* 3rd ed. Published by author: Woodstock; 1986:760–782.

Segre G, Silberberg A. Behavior of macroscopic rigid spheres in Poiseuille flow. *J Fluid Mech.* 1961;14:115–135.

Shekriladze IG. On a possible mechanism for turbulent transition in viscous laminar flow. *Bull Acad Sci Georgian.* 1982;105:277–280.

Vasseur P, Cox RG. The lateral migration of a spherical particle in two-dimensional shear flows. *J Fluid Mech.* 1976;78:385–413.